PNAS
www.pnas.org

Supplementary Information for

Channelrhodopsin-mediated optogenetics highlights a central role of depolarization-dependent plant proton pumps

Reyer, A.[1†], Häßler, M.[1†], Scherzer, S.[1], Huang, S.[1], Pedersen, J. T.[2], Al-Rascheid, K.A.S.[3], Bamberg, E.[4], Palmgren, M.[2], Dreyer, I.[5], Nagel, G.[1,6], Hedrich, R.[1*], Becker, D.[1*]

Becker, D., Hedrich, R.
Email: dirk.becker@uni-wuerzburg.de, hedrich@botanik.uni-wuerzburg.de

This PDF file includes:

Supplementary text
Figures S1 to S8
Tables S1
SI References

Other supplementary materials for this manuscript include the following:

www.pnas.org/cgi/doi/10.1073/pnas.2005626117

Supplementary Information Text

Extended Methods

Plant growth conditions

Nicotiana benthamiana plants were grown in plastic pots on soil (Einheitserde T; Parzer, Germany) in the green house at 26°C in a 16/8 h light/dark photoperiod. Plants were used at the age of 4-5 weeks for Agrobacteria infiltration and impalement measurements. *Arabidopsis thaliana* Col0 ecotype, *Arabidopsis thaliana* Aequorin in Col0 background and *Arabidopsis thaliana* Aequorin ChR2-D156C mutant (ChR2-XXL) in Col0 background were grown in plastic pots (Ø 7 cm) on sterile soil (Einheitserde P; Parzer, Germany) in a climate cabinet at 22°C in a 16/8 h red light/dark photoperiod. To avoid effects of constantly, blue light-activated ChR2-XXL on plant growth, plants were gown under a red light-regime (PHILIPS GP LED production DR 150). The electrophysiological characteristics of plants grown under red light-regime were comparable to control plants grown under white-light regime as their resting potentials were -176 ± 2,4 mV (n=16, SE) and -175.5 ± 3,4 (n=5, SE), respectively. At the age of 5-8 weeks, plants were used for impalement experiments.

MolecularBiology

Genomic DNA (gDNA) was extracted from 6-week-old *A. thaliana* leaves according to Edwards et al. (1). For RNA extraction from 6-week-old *A. thaliana* whole leaf or guard cell enriched epidermal fragments (1) the NucleoSpin® RNA Plant Kit (Macherey-Nagel, Germany) was used following the manufactures instructions. Two micrograms of RNA were used to generate cDNA employing the Moloney Murine Leukemia Virus Reverse Transcriptase (M-MLV RT, Promega). Verification of ChR2-XXL presence in *A. thaliana* PCR on gDNA and cDNA from whole leaf and guard cells was performed using the DreamTaq™ Polymerase (Thermo Fisher Scientific) and the primers ChR2USER fwd: 5'-GGCTTAAUATGGATTATGGAGGCGC-3' and YFP-CT-seq-rev: 5'-GGTTTAAUT TACTTGTACAGCTCGTCCATGCCG-3'.

Localization studies

Transient expression of ChR2 variants *Nicotiana benthamiana* leaf cells by infiltration of Agrobacteria harboring ChR2::YFP/PMDC32 plasmid was performed as described previously using the plasma membrane marker remorin 1.3 (AtRem 1.3) as a co-localization marker (2). Analysis of subcellular localization studies were performed by confocal laser scanning microscopy (Leica TCS SP5 II; Leica Mikrosysteme Vertrieb GmbH, Germany). Images were processed and color-optimized using the Leica confocal software and Fiji (3).

Heterologous protein expression, purification and biochemical characterization

Gene constructs for expression of His_6 tagged and C-terminally truncated AHA2 (aha2Δ92) were transformed and expressed in the yeast RS72 strain, which harbors the yeast PM H^+-ATPase (*PMA1*) under control of a galactose-inducible promoter (4). The microsomal fractions were isolated as described (5) and ahaΔ92 was further solubilized and isolated using the His_6 tag as described (6). The ATPase activity was determined by assaying ATP hydrolysis using the Baginski assay (7) and unless otherwise stated assayed in microtiter plates with a total volume of 60 µl in a assay medium containing 50 mM MOPS/MES, 8 mM $MgSO_4$, 5 mM NaN_3, 0.25 mM $NaMoO_4$, 25 mM KNO_3, 2 mM phosphoenolpyruvate and 30 µg ml^{-1} pyruvate kinase from rabbit muscle (Sigma Aldrich, St Louis, MO) as described (8). The assay medium was equilibrated to 30°C, and assays were started by adding ATP and 20 ng purified protein to the assay medium and run for 30 min. The ATPase activity was measured in a pH range from pH 4.7 to pH 8 and with 2 mM ATP. All experiments were performed in triplicates with ± S.E.

Ion flux measurements on mesophyll cells

H^+ and K^+ concentrations were measured noninvasively using ion selective electrodes. Ion-selective electrodes were pulled from borosilicate glass capillaries w/o filament (Ø 1.0 mm, Science Products) with a vertical puller (Narishige Scientific Instrument Lab), baked over night at 220°C and finally silanized with N, N-Dimethyltrimethylsilylamine (Sigma-Aldrich) for 1 hr. H^+-selective electrodes were backfilled with 40 mM KH_2PO_4/ 15 mM NaCl and tip filled with the hygrogen

ionophore I cocktail A (Sigma-Aldrich). Calibration of H^+-selective electrodes was performed at pH 4 and pH 7. For K^+-selective electrodes, potassium ionophore I cocktail A (Sigma-Aldrich) and 100 mM KCl was used. Calibration was performed at 0.1, 1 and 10 mM KCl. Only electrodes that recorded a shift in voltage of 59 mV per 10x change in K-concentration were used. 5- to 6-week-old leaves via double-sided adhesive tape were mounted to the recording chamber. Lower epidermis was removed, and leaf was incubated in buffer based on 0.1 mM KCl, 0.1 mM $CaCl_2$, and 0.2 mM MES, pH 6.0 (Bis-tris propane). Ion selective electrodes were placed in close contact (~5 µm) to the leaf surface. Following adaptation to experimental conditions, a 5s blue light pulse was applied via an optical fiber while ion concentration was measured.

Oocyte recordings

Functional transport characterization was performed in oocytes of the African clawfrog *Xenopus laevis* using two-electrode voltage-clamp additionally to ion flux measurements. Heterologous expression in oocytes has been described before (9). In brief: cRNA of AHA2 or ChR2 was injected into freshly prepared oocytes and after 2-6 days of expression TEVC (two electrode voltage clamp) was performed. In parallel, ion fluxes across the oocyte plasma membrane were measured noninvasively using the SISE (Scanning Ion Selective Electrodes) technique (10, 11). The standard bath solution for combined TEVC and ion flux measurements contained 0.1 mM KCl, 0.1 mM $CaCl_2$, and 0.2 mM MES/BTP, pH 6.0. The osmolality of solutions was adjusted to 220 mOsm/kg using D-sorbitol. Ion-selective electrodes were prepared as described above and positioned using using an upright microscope (Axioskop, Carl Zeiss AG) and a SM-17 Micromanipulator (Narishige Scientific Instrument Lab) at approx. 5 µm distance to the oocyte equator. Electrodes were connected via Ag/AgCl half-cells to head stages (Applicable Electronics, USA) of an Ion/ Polarographic Amplifier (Applicable Electronics, USA). Electrodes scanned the oocyte at 10 s intervals between two positions with a distance of 100 µm, using a micro-stepping motor driver (US Digital, USA). Raw data were acquired with a NI USB 6259 interface (National Instruments), using custom-built Labview-based software "Ion Flux Monitor." Raw voltage data were converted offline into ion flux data, as described previously (9, 11).

Mathematical description of the voltage- and pH-dependence of the H^+-ATPase.

The pump cycle shown in **Figure S6A** is represented by 6 different conformational states. Its dynamics can be described mathematically by an equation of the type $d\vec{p} = dt \cdot \boldsymbol{Q} \cdot \vec{p}$ with a 6 × 6 ***Q***-matrix. The different entities of the probability vector $\vec{p}$ describe the probabilities to find the system in one of the six states. Its time-dependent variation is determined by the following linear differential equation system:

$$\frac{d\vec{p}}{dt} = \begin{pmatrix} -H_i - k_{16} & k_{21} & 0 & 0 & 0 & k_{61} \\ H_i & -k_{23} - k_{21} & k_{32} & 0 & 0 & 0 \\ 0 & k_{23} & -V_+ - k_{32} & V_- & 0 & 0 \\ 0 & 0 & V_+ & -k_{45} - V_- & H_e & 0 \\ 0 & 0 & 0 & k_{45} & -k_{56} - H_e & k_{65} \\ k_{16} & 0 & 0 & 0 & k_{56} & -k_{61} - k_{65} \end{pmatrix} \cdot \vec{p}$$

Equation (A1)

with the voltage-dependent reaction rates $V_+ = \frac{kT}{h} \cdot k_+ \cdot e^{-\frac{F}{RT}\delta \cdot V}$ and $V_- = \frac{kT}{h} \cdot k_- \cdot e^{-\frac{F}{RT}(1-\delta) \cdot V}$ (*k:* Boltzmann constant, *h*: Planck constant, *T*: absolute Temperature, 0<δ<1, k_+, k_-: constants). The pump usually acts under state-state conditions ($d\vec{p}_{SS}/dt = 0$). In this case, the current transported across the membrane by *N* H^+-ATPase proteins is proportional to the difference between the transition ③→④ and the transition ④→③ (**Fig. S6A**):

$$I_{pump}(V) = N \cdot e_0 \cdot (V_+ \cdot p_{SS}[3] - V_- \cdot p_{SS}[4])$$

Equation (A2)

with N being the number of active pumps in the membrane, the elementary charge e_0, and the steady-state probabilities $p_{SS}[3]$ and $p_{SS}[4]$ for the states ③ and ④, respectively. Solving the equation systems results in an equation of the type:

$$I_{pump}(V) = I_0 \cdot \frac{1 - \frac{[H^+]_{ext}}{[H^+]_{int}} \cdot e^{-\left(\frac{V}{25mV}+A\right)}}{1+e^{-\left(\frac{V}{25mV}+B\right)}+e^{-\left(D\cdot\frac{V}{25mV}+C\right)}}$$

Equation (A3)

The parameter D is a number between 0 and 1, while the parameters I_0, A, B, and C depend in a complex manner on the cytosolic ATP and ADP concentrations and partially (I_0) on the internal and external proton concentrations. In particular the parameter A reflects the energy status of the cell. It determines the value V_{rev} at which the pump current is zero:

$$V_{rev} = \frac{RT}{F} \cdot \left(\ln \frac{[H^+]_{ext}}{[H^+]_{int}} - A\right)$$

Equation (A4)

At this voltage, the energy from ATP-hydrolysis equals the electrochemical transmembrane proton gradient that the proton ATPase has to overcompensate when pumping:

$$\Delta G(V_{rev}) = \left[RT \cdot \ln\left(\frac{[H^+]_{int}}{[H^+]_{ext}}\right) + F \cdot V_{rev}\right] + RT \cdot \ln\left(\frac{K_{ATP}\cdot[ATP]}{[ADP]\cdot[P_i]}\right) = 0$$

Equation (A5)

$$\Rightarrow A = \ln\left(\frac{K_{ATP}\cdot[ATP]}{[ADP]\cdot[P_i]}\right)$$

Equation (A6)

with the apparent equilibrium constant for ATP hydrolysis K_{ATP} (12).

Under usual conditions without fluctuations in the cytosolic ATP and ADP concentrations A, B, and C are just constant numbers. Thus, the dependency of the pump current, which is proportional to the initial Pi production rate, on the internal and external proton concentration and on the membrane voltage is described by

$$I(V) = I_{max} \cdot \underbrace{\frac{1}{1+10^{(pK_e-pH_{ext})}}}_{\substack{pH_{ext}-dependence\\ of\ the\ cycle}} \cdot \underbrace{\frac{10^{(pK_i-pH_{int})}}{1+10^{(pK_i-pH_{int})}}}_{\substack{pH_{int}-dependence\\ of\ the\ cycle}} \cdot \underbrace{\frac{1 - \frac{[H^+]_{ext}}{[H^+]_{int}} \cdot e^{-\left(\frac{V}{25mV}+A\right)}}{1+e^{-\left(\frac{V}{25mV}+B\right)}+e^{-\left(D\cdot\frac{V}{25mV}+C\right)}}}_{\substack{voltage-dependence\\ of\ the\ cycle}}$$

Equation (A7)

Supplementary Figures

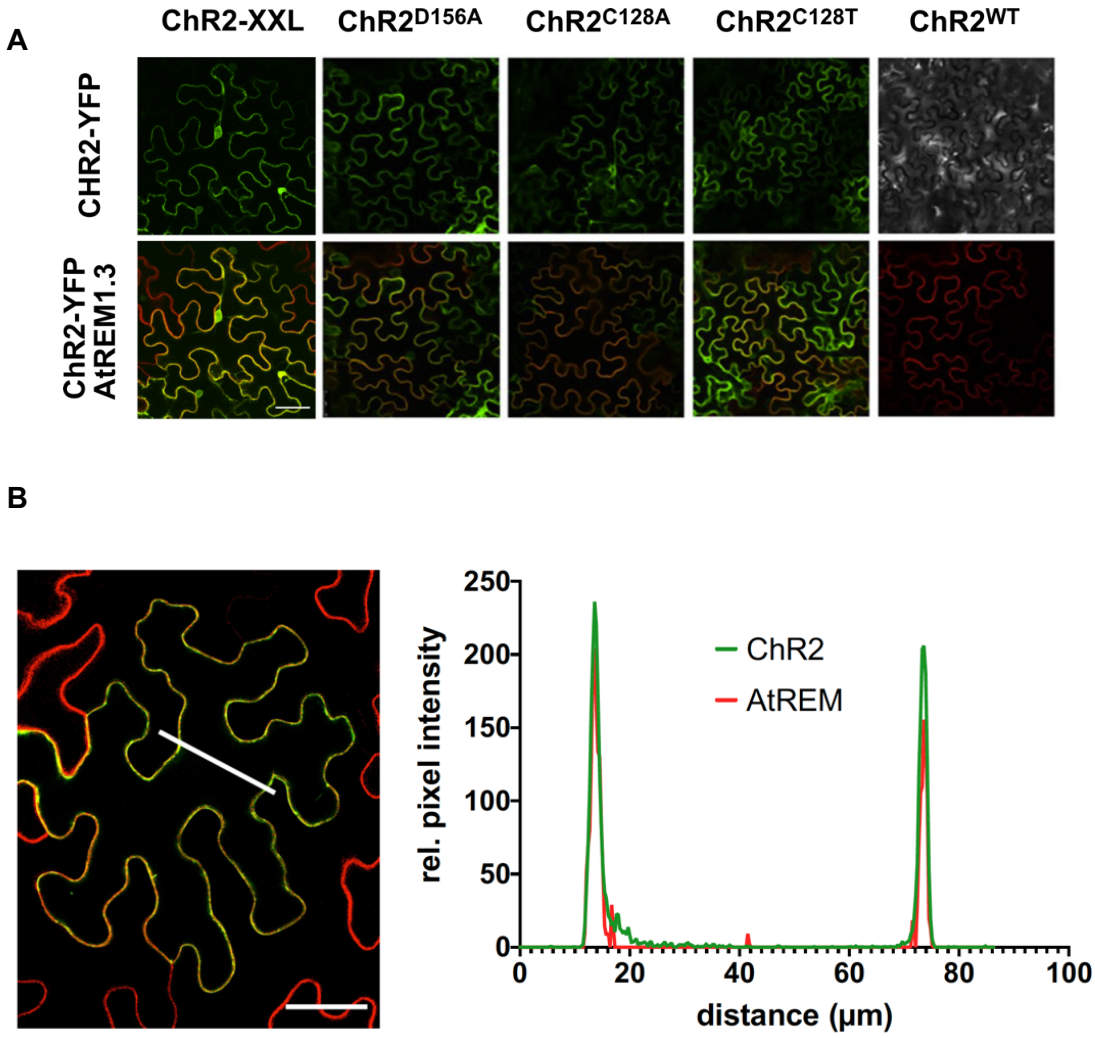

Figure S1. Transient expression of ChR2 in *Nicotiana benthamiana*

(A) Localization of ChR2 variants and ChR2 wild-type fused to YFP upon co-expression with the plasma membrane marker DsRed2::AtREM1.3 in *N. benthamiana* epidermal cells. Microscopic analyses of transiently transformed *N. benthamiana* epidermal cells were performed 2-3 days after infiltration. Colocalization analysis revealed that all ChR2-variants localized to the plasma membrane, while expression was never observed for ChR2 wild-type. (B) Colocalization, line-scan analysis of ChR2-XXL::YFP and DsRed2::AtREM1.3.

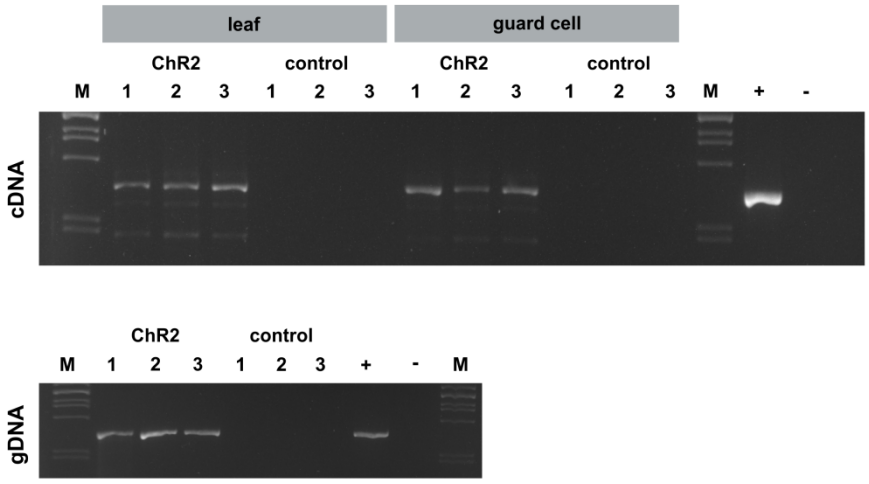

Figure S2. Molecular analysis of stable, ChR2-XXL expressing *Arabidopsis thaliana* plants

Transcriptional (A) and genomic (B) verification of *A. thaliana* (Col-0-Aequorin) plants stably expressing ChR2-XXL. (A) PCR on cDNA of isolated mRNA from leaves and guard cells of three different *A. thaliana* plants. cDNA from the genetic background of ChR2-XXL plants, *A. thaliana* Col-0 expressing aequorin, was used as control. A typical PCR product of 1000 bp was amplified for all ChR2-XXL plant samples in leaves and guard cell samples, but not from *A. thaliana* control samples. ChR2-XXL/plasmid and PCR master mix with water served as a positive control (+) and negative control, respectively. (B) Total genomic DNA from the same plants as in (A) was isolated and used for control-PCR as before. PCR products of 1000 bp were detected for ChR2-XXL plants, but not for the *A. thaliana* aequorin plants. Positive and negative controls were performed as before in (A). The data showed that ChR2-XXL was integrated in the genome and expressed in leaves, as well, as in guard cells of *A. thaliana* ChR2-XXL plants.

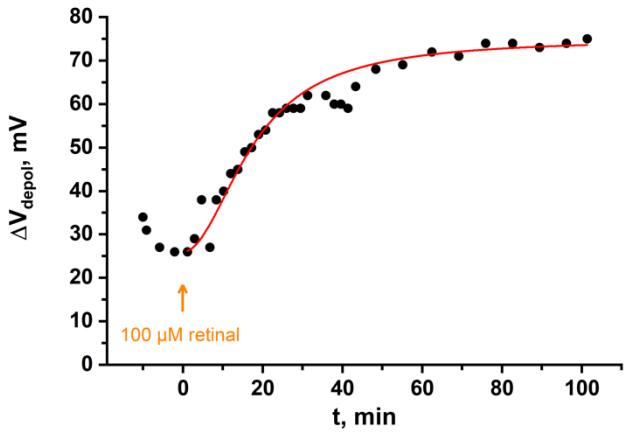

Figure S3. Kinetics of ChR2-XXL reconstitution by retinal

In a continuous impalement recording of mesophyll cells of *A. thaliana* ChR2-XXL, without retinal pretreatment, the maximum depolarization after 5 s blue light were measured every 3 to 4 minutes. After 10 minutes all-trans retinal (100 µM) was added without disruption of the continuous impalement recording. The maximum depolarization after 5 s blue light were measured again every 2 to 3 minutes and after 50 minutes of total recording time in longer periods of 5 to 8 minutes. The increase of amplitude after the addition of retinal was fitted with a Hill Equation and it took about 2 h to reconstitute full channel activity following retinal application.

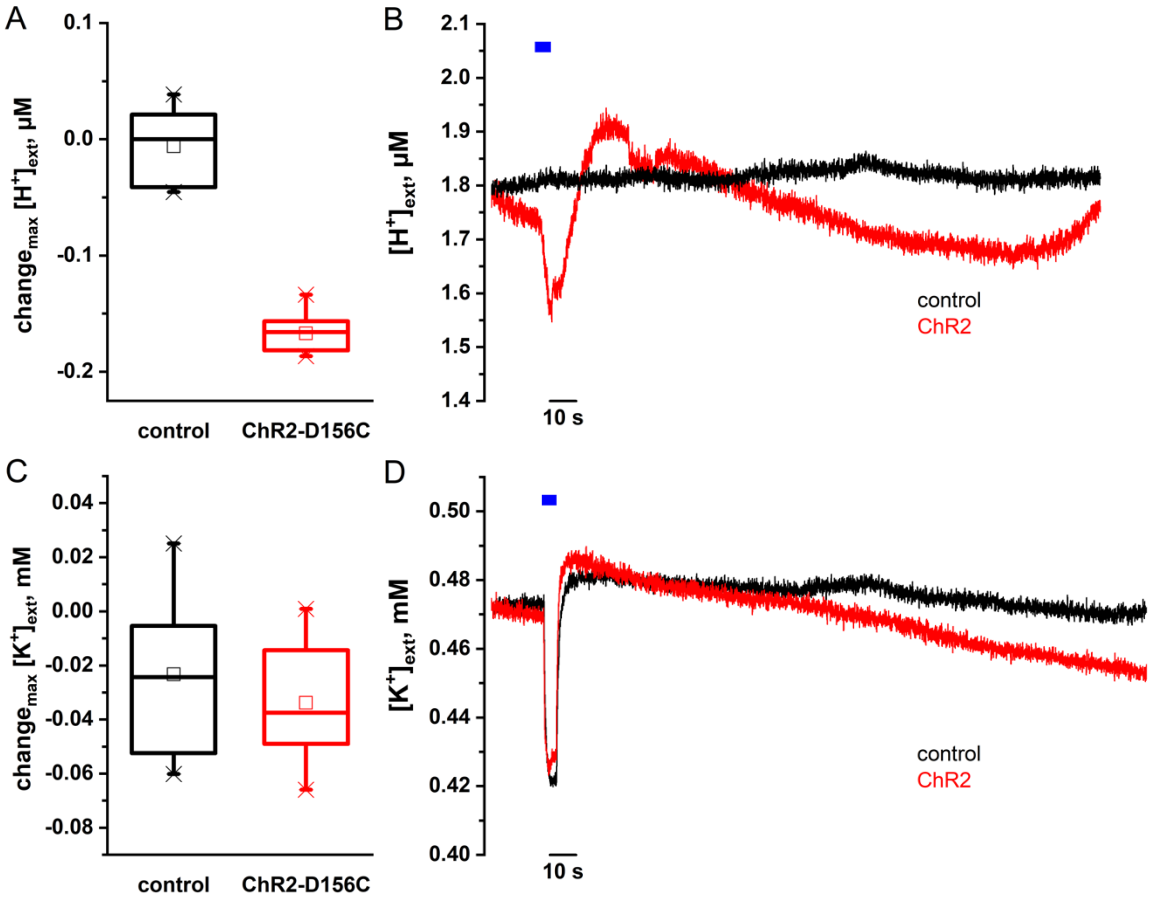

Figure S4: Ion concentration measurements

(A) Apoplastic proton concentration was measured using ion selective microelectrodes. Light induced change in H^+ concentration was investigated for controls (Col-0 Aequorin, black) and ChR2-XXL plants (red). While in control plants 5 s blue light illumination did not change the external H^+ concentration, in ChR2-XXL plants a significant drop in the apoplastic H^+ concentration was observed. (B) Right panels represent representative recordings of data depicted in the left panels. Bottom and top of the boxes denote the first and third quartiles, respectively, the middle line is the median, the whiskers are the most extreme values within 1.5-times the interquartile distance below the first or above the third quartile, crosses indicate the 1st and 99th percentiles ($P = 6.3 \times 10^{-8}$; $F_{1,17} = 144.8$, one-way ANOVA, $n = 9$ different leaves each). (C) Apoplastic K^+ concentration recordings under the same experimental conditions as in (A and B). Different to (A and B) no significant difference between light induced external K^+ concentration was determined between controls (Col-0 Aequorin) and ChR2-XXL plants. The observed blue-light induced transients represent an intrinsic light-sensitivity of the K^+-selective cocktail and do not display a K^+ influx into the cells ($P = 0.4$; $F_{1,19} = 0.7$, one-way ANOVA, $n = 10$ different leaves each). (D) Right panels represent representative recordings of data depicted in the left panels. Blue bar denotes the duration of the blue light-pulse.

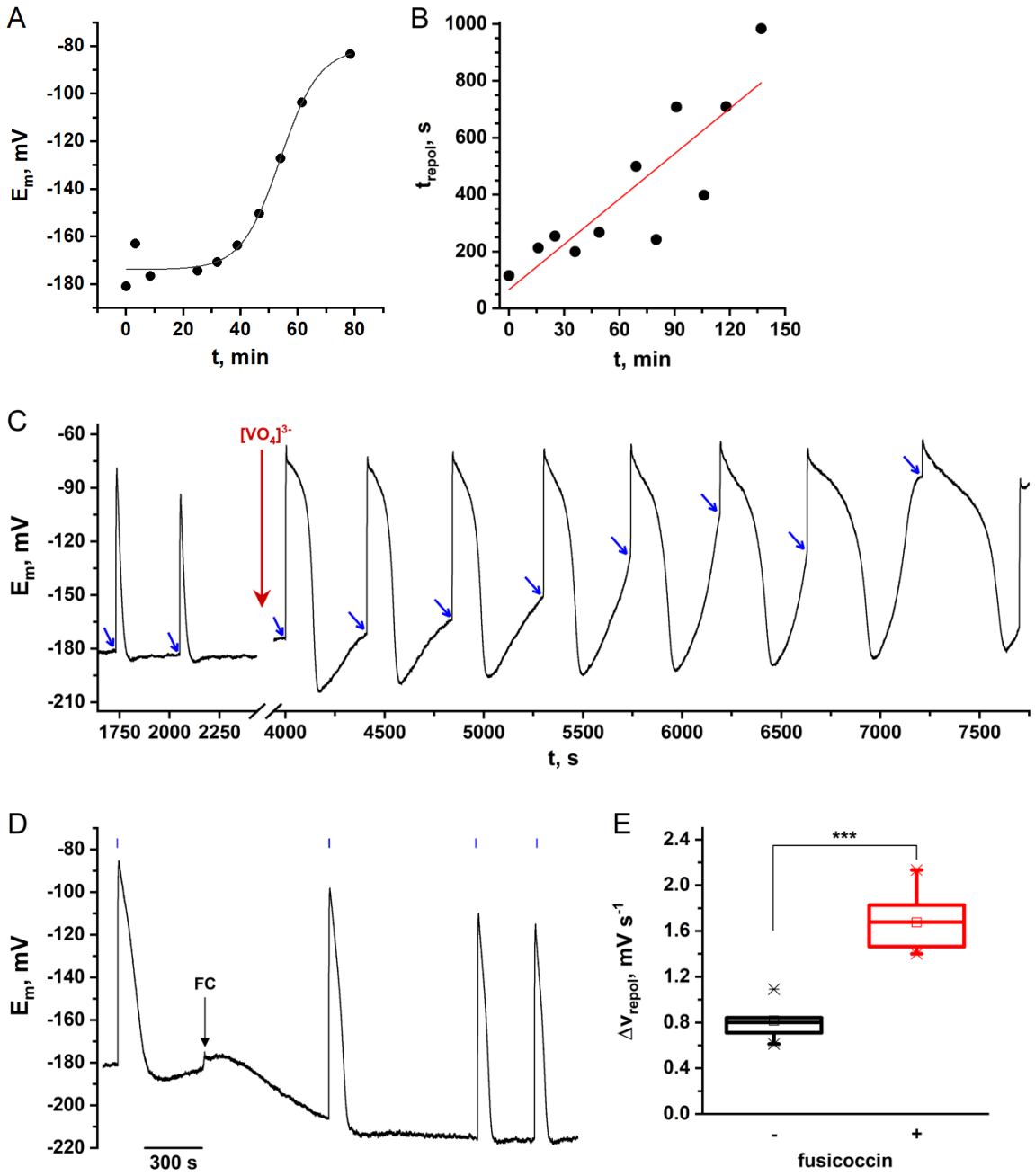

Figure S5: Effect of vanadate and fusicoccin on membrane potential and H^+-pump activity. (A) Effect of the PM H^+-ATPase inhibitor vanadate on the mesophyll resting membrane potential calculated from a representative continuous recording as shown in (C). (B) Effect of vanadate on the duration of the repolarization phase calculated from a representative continuous recording as shown in (C). (C) Representative continuous membrane potential recording in response to the PM H^+-ATPase inhibitor vanadate. Vanadate-treatment is indicated by red arrow. Data points shown in (A) and (B) represent the time to reach the resting potential value (as determined at t_0) following repeated blue light-induced depolarization (blue arrows). (D) Representative continuous membrane potential recording in response to the PM H^+-ATPase activator fusicoccin (arrow denotes fusicoccin application). (D) Effect of fusicoccin on H^+-ATPase-controlled repolarization speed. Box plot data were derived from n=10 experiments, t-test two-sided, $p<0.005$.

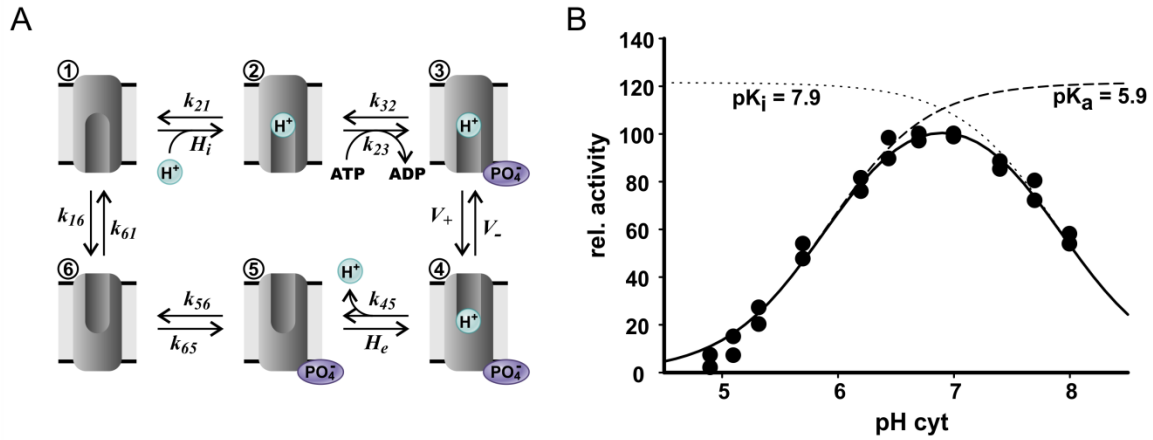

Figure S6. Modeling pH_{cyt}-dependent regulation of H^+-ATPase activity

(A) Proton-pump reaction sequence. In the E1 conformation of the PM H^+-ATPase, substrate H^+ binds to a high affinity binding site of the protein exposed to the cytoplasmic side ($E1 \rightarrow E1H^+$). Phosphorylation by ATP leads to the formation of the E1P intermediate ($E1H^+ \rightarrow E1PH^+$). The phosphorylated protein with the bound proton is less stable and allows the spontaneous transition of the pump to the outward-facing E2P conformation in which the H^+ binding site has reduced affinity ($E1PH^+ \rightarrow E2PH^+$). Concomitantly, the bound H^+ is released from its low affinity binding site ($E1PH^+ \rightarrow E2P$) and the pump gets dephosphorylated ($E2P \rightarrow E2$). The protein without phosphate and proton is more stable in the initial E1 conformation ($E2 \rightarrow E1$). The cycle can start again. The clockwise direction of the cycle is triggered by the phosphorylation step. (B) pH dependence of H^+-ATPase activity. ATP hydrolytic activity of aha2Δ92 as a function of the pH in the test solutions was determined experimentally as described (•). Please note that under the chosen experimental conditions the adjusted pH is present on both sides of the membrane, which allows to determine the dependency on pHcyt and pHext in just one experiment. Experimental data were fitted with the pH-dependent part of equation (A7) considering the experimental constrain of $pH_{ext} = pH_{int} = pH_{solution}$. The gray dotted line (···) depicts the stimulating effect of $[H^+]_{cyt}$ on pump activity (pKi=7.9), while the black dotted line (---) represents the inhibitory effect of $[H^+]_{ext}$ on the pump cycle (pKa=5.9). The combination of both effects results in this experimental conditions in a bell-shaped curve (solid black line, –).

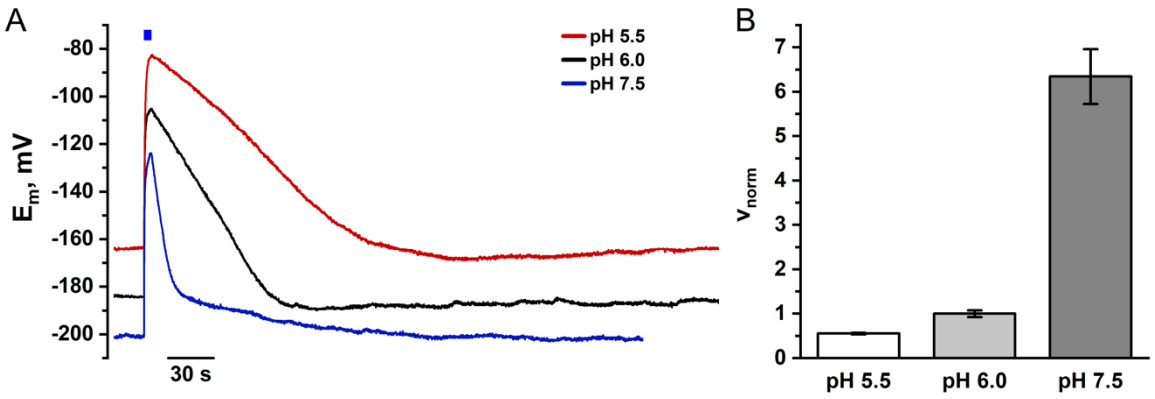

Figure S7. Effect of the proton gradient on PM H^+-ATPase mediated repolarization kinetics
(A) Representative membrane potential recordings of impaled mesophyll cells from the same leaf at different external proton concentrations. Samples were prepared over night without epidermis in bath solution pH 6.0 and pre-incubated for 2 h in bath solutions at indicated pH values before measurement. More acidic conditions at pH 5.5 (red curve) caused a depolarization of the resting potential and elongated the repolarization phase. At more alkaline conditions at pH 7.5 (blue curve) the resting potential was hyperpolarized while repolarization was accelerated in the first 70 % of the total repolarization period. Around -180 mV the repolarization velocity slowed down until the resting potential was reached. We could not observe a hyperpolarization at the alkaline conditions. (B) Repolarization velocity at different external pH conditions. External pH affected the repolarization velocity in the first 70 % of the repolarization phase. The repolarization velocity of five different plants were measured at pH 5.5, 6.0 and 7.5 and then normalized to the repolarization velocity of the corresponding sample at pH 6.0. At pH 5.5 the repolarization velocity changed 0.5-fold compared to pH 6.0. In contrast at pH 7.5 the repolarization velocity was 6.3 times higher compared to pH 6.0.

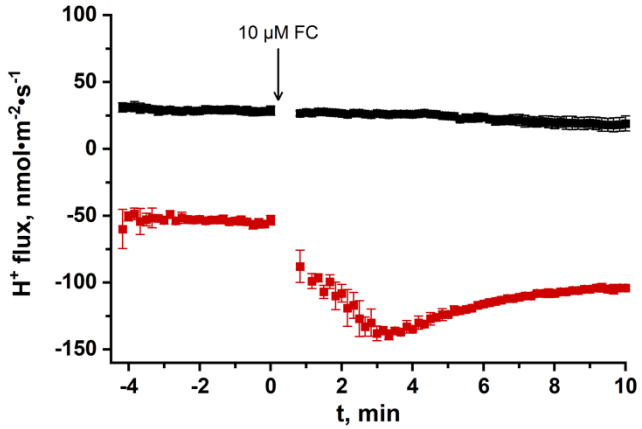

Figure S8: Effect of Fusicoccin on oocyte expressed PM H^+-ATPase activity.
Oocytes injected with water (black) and WT AHA2 RNA (red) were voltage-clamped to 0 mV and H^+-fluxes were recorded using the SISE-technique. Compared to control oocytes, AHA expressing oocytes showed a clear H^+-efflux which was further increased by application of 10 µM fusicoccin to the bath solution (mean ± SD, n≥4).

Table S1. Kinetic properties of ChR2 variants following functional, transient expression in *N. benthamiana* mesophyll cells.

ChR2 mutant in *N. benthamiana*	ΔV_{mean} (mV)	t_{repol} (s)	v_{repol} ($mV \bullet s^{-1}$)
$ChR2^{C128T}$	66 ± 2	27 ± 2	-2.6 ± 0.15
$ChR2^{C128A}$	82 ± 1	198 ± 10	-0.43 ± 0.02
$ChR2^{D156A}$	70 ± 3	1533 ± 171	-0.05 ± 0.01
$ChR2^{D156C}$	107 ± 4	222 ± 14	-0.49 ± 0.002

SI References

1. K. Edwards, C. Johnstone, C. Thompson, A Simple and Rapid Method for the Preparation of Plant Genomic DNA for PCR Analysis. *Nucleic Acids Res.* **19**, 1349-1349 (1991).
2. F. Demir *et al.*, Arabidopsis nanodomain-delimited ABA signaling pathway regulates the anion channel SLAH3. *Proc. Natl. Acad. Sci. U. S. A.* **110**, 8296-8301 (2013).
3. J. Schindelin *et al.*, Fiji: an open-source platform for biological-image analysis. *Nature Methods* **9**, 676-682 (2012).
4. A. Cid, R. Perona, R. Serrano, Replacement of the promoter of the yeast plasma membrane ATPase gene by a galactose-dependent promoter and its physiological consequences. *Curr. Genet.* **12**, 105-110 (1987).
5. A. G. Wielandt *et al.*, Specific Activation of the Plant P-type Plasma Membrane H^+-ATPase by Lysophospholipids Depends on the Autoinhibitory N- and C-terminal Domains. *J. Biol. Chem.* **290**, 16281-16291 (2015).
6. J. T. Pedersen, T. Kanashova, G. Dittmar, M. Palmgren, Isolation of native plasma membrane H^+-ATPase (Pma1p) in both the active and basal activation states. *FEBS Open Bio* **8**, 774-783 (2018).
7. E. S. Baginski, P. P. Foa, B. Zak, Microdetermination of inorganic phosphate, phospholipids, and total phosphate in biologic materials. *Clin. Chem.* **13**, 326-332 (1967).
8. J. T. Pedersen, J. Falhof, K. Ekberg, M. J. Buch-Pedersen, M. Palmgren, Metal Fluoride Inhibition of a P-type H^+ Pump: Stabilization of the Phosphoenzyme Intermediate Contributes to Post-Translational Pump Activation. *J. Biol. Chem.* **290**, 20396-20406 (2015).
9. J. Böhm *et al.*, Understanding the Molecular Basis of Salt Sequestration in Epidermal Bladder Cells of *Chenopodium quinoa*. *Curr. Biol.* **28**, 3075-3085 e3077 (2018).
10. J. Böhm *et al.*, The Venus Flytrap *Dionaea muscipula* Counts Prey-Induced Action Potentials to Induce Sodium Uptake. *Curr. Biol.* **26**, 286-295 (2016).
11. J. Dindas *et al.*, AUX1-mediated root hair auxin influx governs $SCF^{TIR1/AFB}$-type Ca^{2+} signaling. *Nat Commun* **9**, 1174 (2018).
12. F. Rienmuller *et al.*, Luminal and cytosolic pH feedback on proton pump activity and ATP affinity of V-type ATPase from *Arabidopsis*. *J. Biol. Chem.* **287**, 8986-8993 (2012).